

Hoai Nam Le ¹, Phuoc Vinh Dang ¹, Anh-Duc Pham ¹,
Nhu Thanh Vo ¹

System identifications of a 2DOF pendulum controlled by QUBE-servo and its unwanted oscillation factors

System identification is an approach for parameter detection and mathematical model determination using response signals of a dynamic system. Two degrees of freedom (2DOF) pendulum controlled by a QUBE-servo motor is a great experiment device to work with; though it is not easy to control this system due to its complex structure and multi-dimensional outputs. Hence, system identification is required for this system to analyze and evaluate its dynamic behaviors. This paper presents a methodology for identifying a 2DOF pendulum and its dynamic behaviors including noise from an encoder cable. Firstly, all parameters from both mechanical and electrical sides of the QUBE-servo motor are analyzed. Secondly, a mathematical model and identified parameters for the 2DOF pendulum are illustrated. Finally, disturbances from encoder cable of the QUBE-servo motor which introduce an unwanted oscillation or self-vibration in this system are introduced. The effect of itself on output response signals of the 2DOF QUBE-pendulum is also discussed. All identified parameters are checked and verified by a comparison between a theoretical simulation and experimental results. It is found that the disturbance from encoder cable of the 2DOF QUBE-pendulum is not negligible and should be carefully considered as a certain factor affecting response of system.

1. Introduction

System identification is an approach for parameters detection and mathematical model determination by using response signals of a dynamic system [1, 2]. The process of system identification includes two steps, collecting response signals

✉ Nhu Thanh Vo, e-mail: vnthanh@dut.udn.vn

¹Faculty of Mechanical Engineering, The University of Danang – University of Science and Technology, Danang, Vietnam.



© 2020. The Author(s). This is an open-access article distributed under the terms of the Creative Commons Attribution-NonCommercial-NoDerivatives License (CC BY-NC-ND 4.0, <https://creativecommons.org/licenses/by-nc-nd/4.0/>), which permits use, distribution, and reproduction in any medium, provided that the Article is properly cited, the use is non-commercial, and no modifications or adaptations are made.

of the system in either time or frequency domain and estimating the adjustable parameters of that system with a predicted mathematical model [3, 4]. Moreover, this process also comprises an optimal design of experimental data for efficiently generating parameter information of the system. The goals of system identification are mathematical relations between behavior and inputs of the system without going into much detail of the system's dynamics [5, 6]. For example, system identification can be applied to recognize the controllability matrix and observability matrix of a system or to perceive the failure of sensors and actuators [7]. In addition, system identification is an important process to detect unknown external disturbances affecting system response [8, 9]. Obviously, system identification can both improve the quality of controller design and help to clearly understand physical phenomena happening in the system.

In fact, a 2DOF pendulum that operates on a rotary platform of K. Furuta is a genuine model to study not only control methods but also system identification. For instance, some researches on nonlinear sliding mode control and predictive control were applied in this type of pendulum with simulated models [10, 11]. Furthermore, experimental results of the designed controller used in swing-up term of pendulum is also illustrated to verify the proposed control methods [12–14]. Validation to confirm the effectiveness of several swing-up controls can be determined based on swing-up periods [15]. Recently, an upgraded version for the Furuta pendulum was presented with a double-inverted pendulum arm [16]. However, to successfully control the 2DOFs pendulum model of Furuta, all parameters and external impacts to operation of the pendulum have to be collected and verified with system identification [16, 17].

Besides, a 2DOF pendulum controlled by a QUBE-servo motor is a good choice for the experimental activities for system identification. However, this device has a complicated structure and multi-dimensional outputs, resulting in difficulty in controlling the system [18]. The 2DOF rotary pendulum attached to the coreless brushed DC servo motor of Quanser provider is an excellent device for controls topics [19–23]. In general, one 2DOF QUBE-pendulum comprises a rotating pendulum arm magnetically fixed on the vertical rotating shaft of DC servo motor as shown in Fig. 1. An external encoder with long-distance cable is used to measure the rotational angle of the pendulum. Up to date, several works have been done with this test-rig device. First of all, Kathpal from India [19] used a toolbox in MATLAB, SimMechanics, to build a simulation model for LQR control techniques of QUBE-pendulum. In [20], D.L. Peters tried to develop a new platform for an example of both the second-underdamped model and Ziegler-Nichols PID tuning on the QUBE-system. Moreover, parameter identification of DC motor of the QUBE system using inertia is simulated and validated by experimental results [21, 22]. Lastly, in Krishnan's dissertation [23], a completed non-linear control of 2DOF pendulum controlled by the QUBE-servo motor is illustrated and validated with its estimated parameters. However, all previous researches did not distinguish between the sources of external disturbances and did not evaluate the influence

of encoder cable of pendulum on response of QUBE system. Due to this lack of information, system identification that considers the effect of encoder cable of pendulum is required for QUBE system to analyze and evaluate its dynamic behavior.

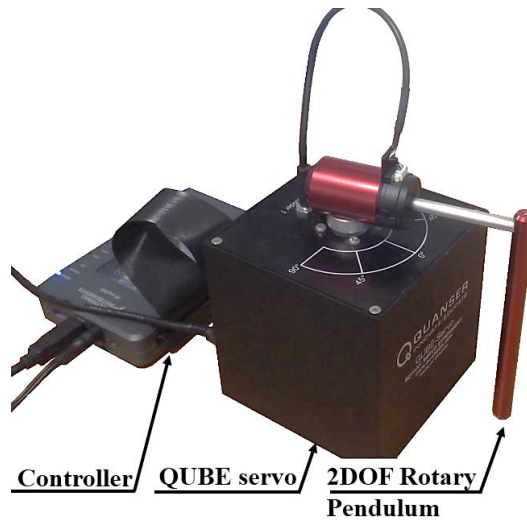


Fig. 1. Test rigs of 2DOF pendulum controlled by the QUBE-servo

This paper presents a methodology for identifying a 2DOF pendulum and its dynamic behaviors including noise from the encoder cable. At the first step, all parameters from both electrical and mechanical sides of a DC servo motor delivered by Quanser provider are evaluated. Next, a mathematical model and identified parameters for the 2DOF pendulum are described. Finally, the disturbances from encoder cable of the QUBE-servo motor making an unwanted oscillation or self-vibration in this system are introduced, and the effect of itself to output response signals of the 2DOF QUBE-pendulum is also discussed. All the collected parameters of identification are checked and verified by a comparison between a theoretical simulation and experimental results.

2. Introduction of test-rig

A diagram of 2DOF pendulum controlled by the QUBE-servo motor and its control system are illustrated in Fig. 2. Based on the structure of this model, the vertical DC motor makes an oscillation of a pendulum link, which is connected to the output-shaft of the motor by a pendulum arm. Motor and pendulum angles are measured by two high-precision encoders. Command input for the motor and the data of motor encoder is given by a controller named NI-myRio through a DAQ board and a PWM amplifier. However, a cable is used to connect the pendulum

encoder with the DAQ board for acquiring data. This cable has an unwanted effect on collected results from the angular movement of pendulum at the output. Hence, with this structure model, the process of system identification can be divided into three parts: motor identification, pendulum model and effect of unwanted oscillation originating from pendulum encoder cable. Furthermore, information on the control system is shown in Table 1 [18].

Table 1.

Specifications for control system of the 2DOF QUBE-pendulum

NI myRIO Controller	Power Requirement	
	Power supply voltage	6–16 VDC
	Maximum power consumption	14 W
	Analog Input	
	sample rate	500 kS/s
	Resolution	12 bits
	Bandwidth	2–20000 Hz
	Analog Output	
	maximum update rates	345 kS/s
	Resolution	12 bits
	Bandwidth	2–50000 Hz
	Digital I/O	
	Number of lines	1 port of 8 DIO lines
	Logic level	5 V compatible LVTTTL input; 3.3 V LVTTTL output
	Input logic levels	$2.0 V_{\min}$; $5.25 V_{\max}$
Output logic levels	$2.4 V_{\min}$; $3.465 V_{\max}$	
Maximum frequencies for PWM	100 kHz	
QUBE-servo	Dimension (W × L × H)	$10.2 \times 10.2 \times 11.7$ cm
	Overall mass	1.2 kg
	Pendulum mass	0.1 kg
	Pendulum length	9.5 cm
	Motor and pendulum encoder resolution (non-quadrature decoding)	512 counts/revolution
	Motor input voltage	18 VDC
	Motor nominal current	0.54 A
	DC motor nominal speed (no load)	4050 rpm

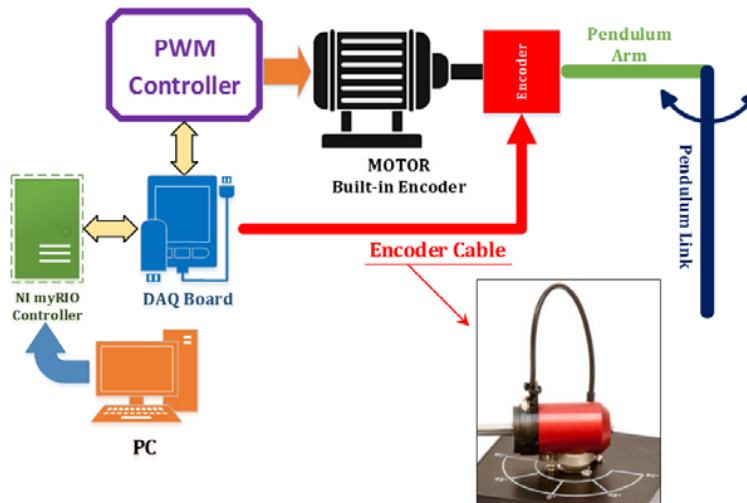


Fig. 2. Experimental diagram of 2DOF pendulum controlled by the QUBE-servo

3. System identification

3.1. DC servo motor identification

A DC servo motor is an electro-mechanical system which directly provides a rotary motion in the system [24]. The equivalent circuit and free-body diagram of the QUBE-servo motor are shown in Fig. 3. Basically, this armature circuit consists of the internal electric resistance R_m and inductance L_m . The armature current i_m of the motor is generated in this circuit by an input voltage source V_m , then transferred to the motor torque T_m as output. Moreover, position θ_m and speed $\dot{\theta}_m$ of the QUBE-servo motor shaft depend on changes of the applied input voltage V_m .

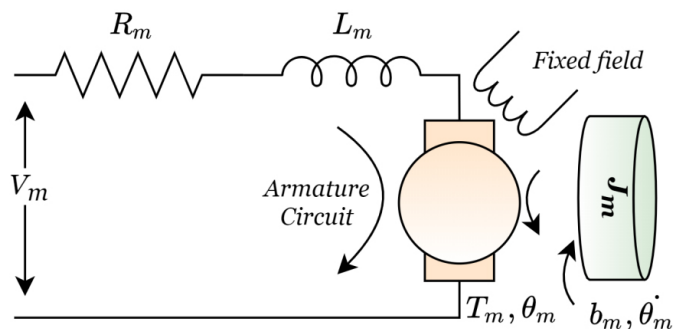


Fig. 3. Equivalent circuit and free-body diagram of the QUBE-servo motor

The mathematical model of this QUBE-servo motor is illustrated in Eq. (1) based on Kirchoff's Voltage Law and Newton's Second Law for one electro-mechanical system.

$$\begin{aligned} J_m \ddot{\theta}_m + b_m \dot{\theta}_m &= K_t i_m, \\ L_m \frac{di_m}{dt} + R_m i_m &= V_m - K_m \dot{\theta}_m. \end{aligned} \quad (1)$$

The term $L_m(di_m/dt)$ is negligible compared to $R_m i_m(t)$, because of small inductance value. Furthermore, the motor torque K_t and the motor back EMF constant K_m are equal and are the inverse of steady-state gain K . Thus, Eq. (1) can be written as Eq. (2).

$$\begin{aligned} J_m \ddot{\theta}_m + b_m \dot{\theta}_m &= K_m i_m, \\ R_m i_m &= V_m - K_m \dot{\theta}_m. \end{aligned} \quad (2)$$

The relationship between the input – voltage V_m and the output – position (or speed) of motor shaft θ_m (or $\dot{\theta}_m$) is illustrated by Laplace transfer function as Eqs. (3)–(6). Based on it, there are four unknown parameters of this QUBE-servo motor: internal motor resistance R_m , the steady-state gain K , motor viscous friction coefficient b_m , and the total moment of inertia acting on the motor shaft J_m .

$$\frac{\Theta_m(s)}{V_m(s)} = \frac{K_m}{(J_m s + b)R_m + K_m^2}, \quad (3)$$

$$\frac{\dot{\Theta}_m(s)}{V_m(s)} = \frac{K_m}{\tau s + 1} \quad (4)$$

with

$$\tau = \frac{J R_m}{K_m^2}, \quad (5)$$

$$K_m = \frac{1}{K} = \frac{\text{Steady-state output value}}{\text{Input value}}. \quad (6)$$

The internal motor resistance R_m is determined by measurement, whereas motor steady-state gain K , motor viscous friction coefficient b_m , and total moment inertia J_m can be derived from data acquisition of motor response. In particular, the internal resistance of motor R_m in the armature circuit can be measured by a digital multi-meter; and the value of R_m in this used system is 8.4 Ω . However, the value of motor gain and total moment of inertia should be determined based on the response of the output signal of motor shaft, as shown in Fig. 4.

The steady-state gain K (or DC gain) is the ratio between the steady-state value of output (speed) and the input value (voltage), as shown in Fig. 4. Hence, the

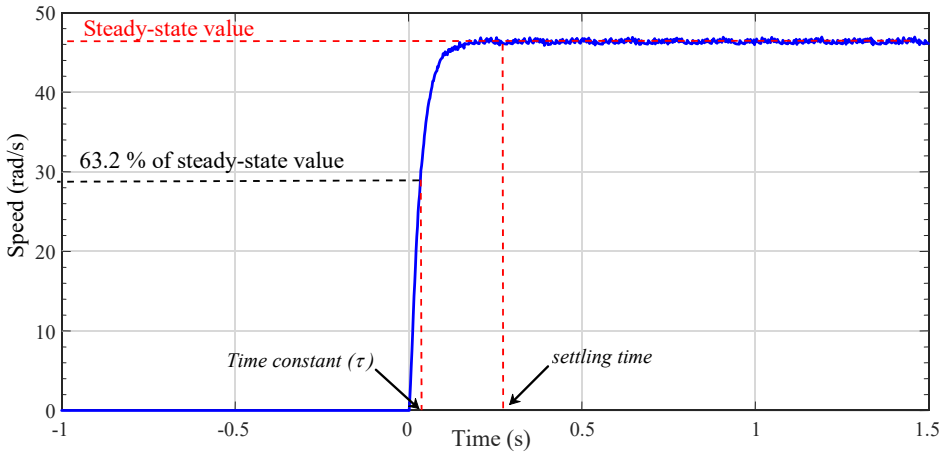


Fig. 4. Settling and steady states of angular velocity of the QUBE-servo motor

motor back emf constant K_m is the inverse of steady-state gain K , $K_m = 0.0431$. Moreover, the total moment of inertia acting on motor shaft J_m can be found by using the value of time constant τ which is a time for response to reach 63.2% final value, internal motor resistance R_m , and motor back emf constant K_m , as shown in Eq. (7), $J_m = 6 \times 10^{-5} \text{ kg m}^2$.

Finally, based on the response of output angular velocity and value of armature current in motor with various values of input voltage as shown in Fig. 5; the motor viscous damping coefficient can be calculated by using Eq. (8). The viscous damping coefficient of the motor is estimated as the average value of current results

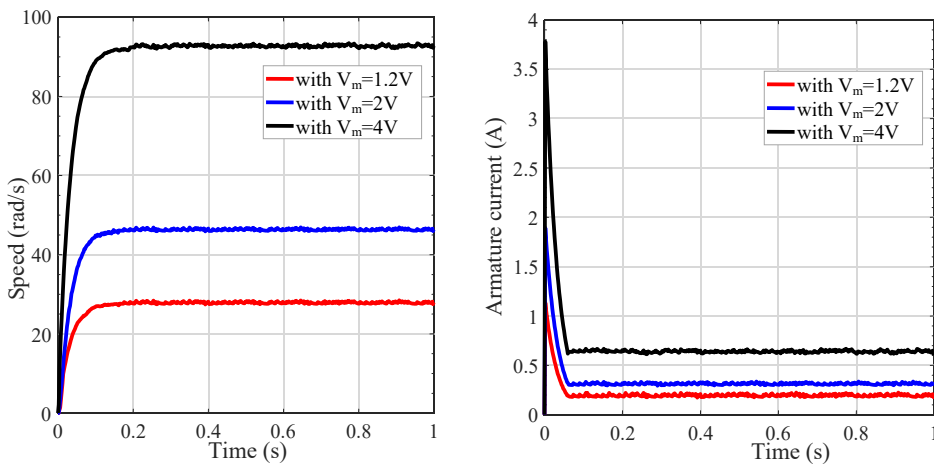


Fig. 5. Response of motor angular velocity (left) and armature current (right) with various input voltages

in the steady-state of motor, $b_m = 3 \times 10^{-4}$ Nm/rad/s.

$$J_m = \frac{\tau K_m^2}{R_m}, \quad (7)$$

$$b_m = \text{average} \left(\sum_{i=1}^n \frac{K_{mi} i_{mi}}{\dot{\theta}_{mi}} \right). \quad (8)$$

3.2. Characteristics of the rotary pendulum

When the pendulum is attached to the motor shaft as shown in Fig. 2, the dynamic system of the rotary pendulum controlled by the QUBE-servo becomes a second-order system. In comparison to the traditional pendulum, whose system base is attached on a limited rail and its movement is made by linear motion, the rotary pendulum uses an unlimited rotation as the input and transfers the movement to the pendulum link. As shown in Fig. 6, the pendulum arm L_A is set in oscillation with an angle θ_m by the QUBE-servo motor which causes an oscillation of pendulum link L_L with an angle θ_L . Based on Euler-Lagrange differential equation, the equations of motion (EOM) for the rotary pendulum are described as Eqs. (9), (10) [13, 15].

$$\begin{aligned} & \left(m_L L_A^2 + \frac{1}{4} m_L L_L^2 - \frac{1}{4} m_L L_L^2 \cos^2 \theta_L + J_A \right) \ddot{\theta}_m - \frac{1}{2} m_L L_L L_A \cos \theta_L \ddot{\theta}_L \\ & + \frac{1}{2} m_L L_L^2 \sin \theta_L \cos \theta_L \dot{\theta}_m \dot{\theta}_L + \frac{1}{2} m_L L_L L_A \sin \theta_L \dot{\theta}_L^2 = T_m - D_A \dot{\theta}_m, \\ & \frac{1}{2} m_L L_L L_A \cos \theta_L \ddot{\theta}_m + \left(J_L + \frac{1}{4} m_L L_L^2 \right) \ddot{\theta}_L - \frac{1}{4} m_L L_L^2 \cos \theta_L \sin \theta_L \dot{\theta}_m^2 \\ & + \frac{1}{2} m_L L_L g \sin \theta_L = -D_p \dot{\theta}_L, \end{aligned} \quad (9)$$

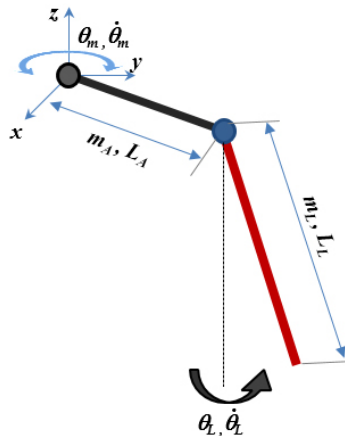


Fig. 6. Free-body diagram for the rotary pendulum

where:

$$T_m = K_m \frac{(V_m - K_m \dot{\theta}_m)}{R_m} : \text{input from motor.} \quad (10)$$

The parameters of this pendulum system can be identified by measurement. First, the weight and length of the pendulum arm and link (m_A, m_L, L_A, L_L) can be collected by using a weight scale and a caliper. The inertia moment of pendulum arm J_A and link J_L can be calculated based on their weight and length, as shown in Eqs. (11), (12), respectively. Moreover, the damping coefficient of pendulum arm D_A is also the viscous damping coefficient of motor b_m ; whereas the damping coefficient of pendulum link D_L , which is the ratio between applied torque and the speed in an individual test of pendulum link, can be checked by using a torque tester such as Helixa-I of Mecmsin or the one provided by the manufacturer of pendulum link, $D_L = 5 \times 10^{-4}$ Nm/rad/s. However, because of its small value, the damping coefficient of pendulum link D_L can be neglected.

$$J_A = \frac{7}{48} m_A L_A^2, \quad (11)$$

$$J_L = \frac{1}{3} m_L L_L^2. \quad (12)$$

A simulation model for the 2DOF pendulum controlled by the QUBE-servo motor is built based on the above identified parameters in MATLAB. The block diagram of simulation model is illustrated in Fig. 7. Generally, the command input with motor angle is transferred through a motor controller and a MATLAB function for solving nonlinear EOM of the rotary pendulum; the data of actual motor angle θ_m and pendulum-link angle θ_L is known at the output. With all identified parameters, we can simulate the vibration response of pendulum and collect characteristics of the 2DOF QUBE rotary pendulum system.

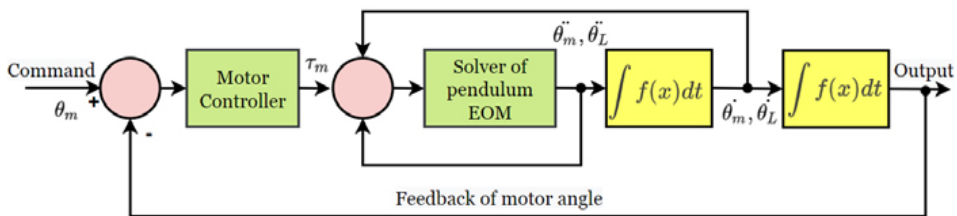


Fig. 7. Simulation model of the 2DOF QUBE rotary pendulum in MATLAB

In fact, the rotary pendulum attached to the QUBE-servo motor has all characteristics of the second-order system. The vibration response of the rotary pendulum is illustrated in Fig. 8. This response shows that the rotary pendulum works as an underdamped system, that moves quickly to the equilibrium. Characteristics of this

underdamped system [25] are determined by the damping ratio and the natural frequency, as shown in Fig. 8. Whereas, the damping ratio ζ_P of the rotary pendulum system can be extracted by using peak-values ($y(t)$, $y(t + nT_d)$) of vibration response with log-decrement method as Eq. (13) (with T_{dP} : time period of the oscillations); the natural frequency ω_{nP} can be calculated from damped natural frequency ω_{dP} and damping ratio ζ_P as Eq. (14).

$$\xi_P = \frac{1}{\sqrt{1 + \left(\frac{2\pi}{\delta_P}\right)^2}} \quad \text{with } \delta = \frac{1}{n} \ln \frac{y(t)}{y(t + nT_d)} : \text{ log-decrement,} \quad (13)$$

$$\omega_{nP} = \frac{\omega_{dP}}{\sqrt{1 - \xi_P^2}} \quad \text{with } \omega_d = \frac{2\pi}{T_d} : \text{ damped natural frequency.} \quad (14)$$

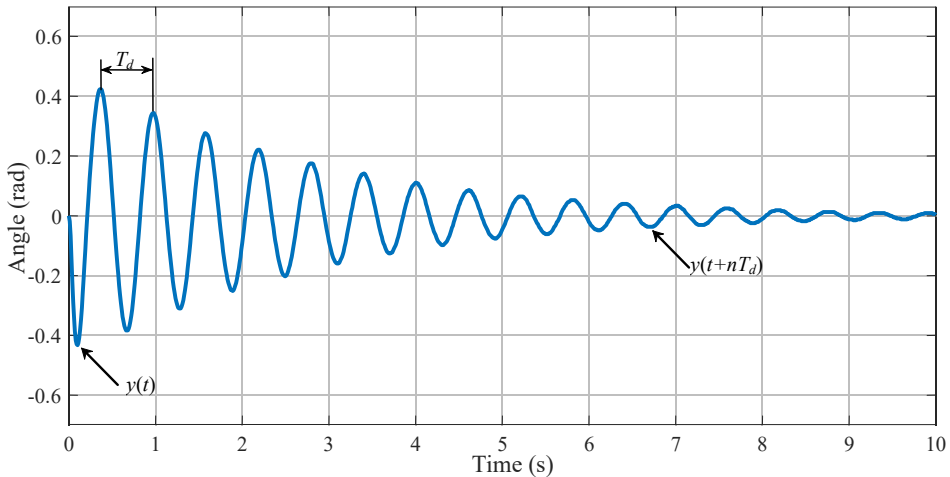


Fig. 8. Response characteristics of the system

3.3. Effect of encoder cable on the response of system and its unwanted oscillation factors

With all identified parameters, the output response of the system for a predicted input should be matched to simulation and experiment results, but there is a difference between them. In fact, this distinction is illustrated in Fig. 9. The comparison results indicate that the oscillation of pendulum link in the 2DOF QUBE rotary pendulum system is longer than its usual one. The simulation result of pendulum vibration with correctly identified parameters in previous sections is shown by the blue-line in Fig. 9. However, this simulation result did not closely match experimentally measured results shown by the red-dashed-line. Evidently, this result is

affected by outer disturbances or un-modeled parameters such as air-friction and elastic deformation, electromagnetic and feedback signal delay of the encoder cable. In that, the effect from encoder cable of pendulum link is the main contributor to this difference.

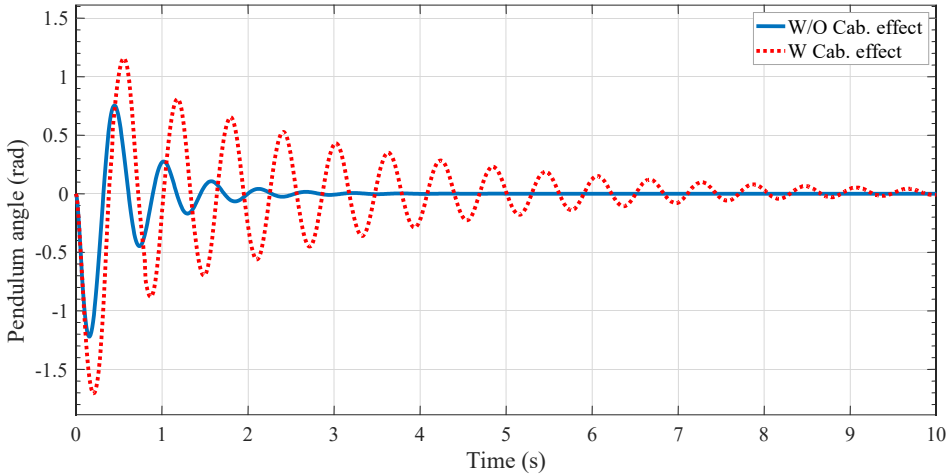


Fig. 9. A comparison between responses of pendulum vibration with and without cable effect

By subtracting time responses resulting from experiment from those of simulation of pendulum oscillation, we show the unwanted effect of the encoder cable, illustrated in Fig. 10. It is clearly seen that the response of the encoder cable oscillation is also a function of second-order system. A transfer function of oscillation response of encoder cable is presented as Eq. (15), with damping ratio of

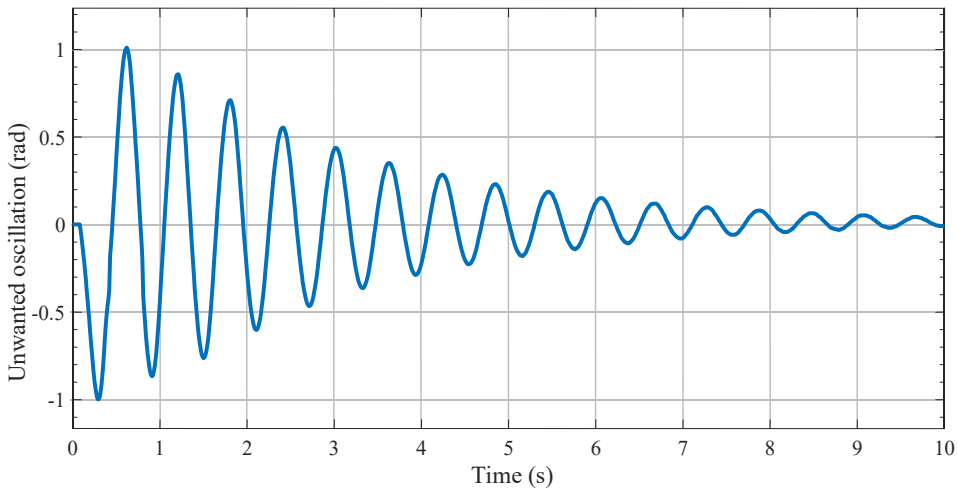


Fig. 10. Unwanted oscillation of encoder cable in the 2DOF QUBE-pendulum

cable oscillation $\xi_{n_cableP} = 0.034$ and its natural frequency $\omega_{n_cableP} = 10.36$ Hz calculated by Eqs. (13), (14), respectively.

$$\frac{\Theta_{cable}(s)}{\Theta_m(s)} = \frac{\omega_{n_cableP}^2}{s^2 + 2\zeta_{cableP} \omega_{n_cableP} s + \omega_{n_cableP}^2}. \quad (15)$$

The encoder cable of the pendulum increases the fluctuation of pendulum link, whereas it reduces the oscillation of the pendulum arm (motor angle). The comparison between motor responses when the QUBE-pendulum model is attached to the encoder cable and when QUBE-pendulum model does not have the encoder cable is shown in Fig. 11. In detail, motor response of the 2DOF QUBE-pendulum having no encoder cable is shown as the blue-line in Fig. 11. This result is verified and validated by both simulation and experiment. Obviously, the motor response or the position response of the pendulum arm in the 2DOF QUBE-pendulum model should also be an underdamped system [20]. However, due to the influence of encoder cable, the motor response of QUBE-pendulum is becoming a response of critically damped system. The difference between responses of the motor having QUBE-pendulum with and without encoder cable is also shown in Fig. 12; then it is estimated as a function using Eq. (16). This equation is a Fourier series for the reduction angle $\theta_{MotorDamp}(t)$ due to the effect of cable on the response of pendulum arm, a function of time t , with the coefficients derived from a spectral analysis in frequency domain of data in Fig. 13. Furthermore, these coefficients are indicated in Table 2.

$$\theta_{MotorDamp}(t) = \sum_{i=1}^n A_i \cos(2\pi f_i t + \varphi_i). \quad (16)$$

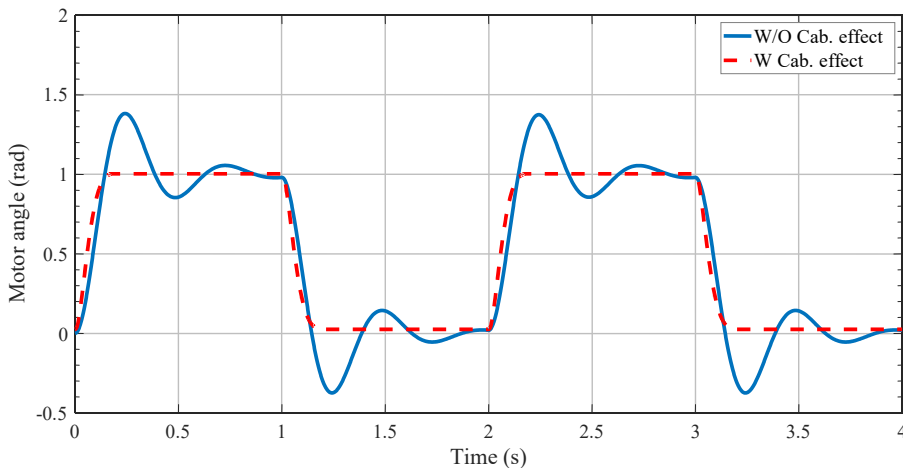


Fig. 11. Comparison of motor responses with and without cable effect

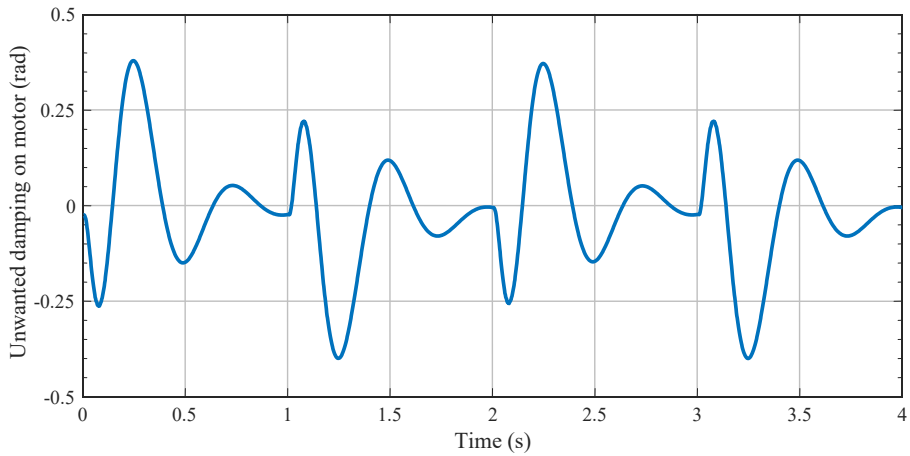


Fig. 12. Unwanted damping on motor affected by encoder cable

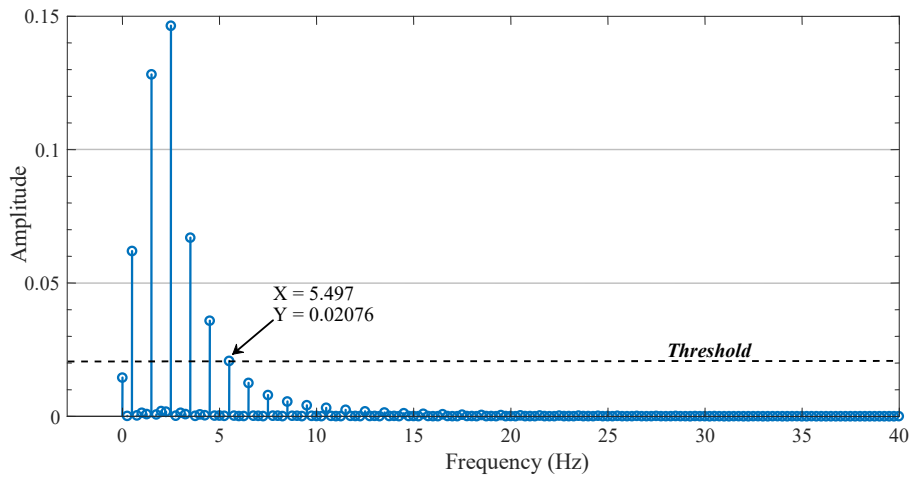


Fig. 13. Frequency analysis for unwanted damping on motor

Table 2.

Estimated Fourier coefficients of unwanted damping due to encoder cable

No	Frequency f_i (Hz)	Amplitude A_i (rad)	Phase ϕ_i (rad)
1	0.4998	0.062	-1.033
2	1.4988	0.128	0.829
3	2.4988	0.1464	-1.122
4	3.4983	0.067	0.972
5	4.4983	0.0359	0.401

4. Conclusions

This paper presents a methodology for identifying a 2DOF pendulum and its dynamic behaviors including the disturbance effect from an encoder cable. All the collected parameters of identification are checked by a comparison between a theoretical simulation and experimental results of the system shown in Table 3. Some conclusions can be drawn from the results, as follows:

1. The output response of the 2DOF QUBE rotary pendulum can be feasibly used to identify parameters of the system. However, the disturbance which occurs an unwanted oscillation inside the QUBE-pendulum system should be carefully considered. One can conclude that this effect cannot be ignored and should be remarkably noted as an important factor which affects to the output responses of system.
2. It should be noted that, while the unwanted damping factor from the encoder cable in the 2DOF QUBE-pendulum system makes the pendulum link more flexible, it reduces the vibration amplitude of the motor.
3. Further works using methods to reduce oscillation of system having the same structure as the 2DOF QUBE-pendulum should include a calculation

Table 3.

Identified parameters of the 2DOF QUBE-pendulum system

Parameters	Symbol	Value and units
Internal resistance of motor	R_m	8.94 Ω
Motor back-emf constant	K_m	0.0431
Total moment of inertia acting on motor shaft	J_m	6×10^{-5} kg m ²
Viscous damping coefficient	b_m	3×10^{-4} Nm/rad/s
Damping coefficient of pendulum arm	D_A	3×10^{-4} Nm/rad/s
Damping coefficient of pendulum link	D_L	5×10^{-4} Nm/rad/s
Weight of pendulum arm	m_A	0.053 kg
Weight of pendulum link	m_L	0.024 kg
Length of pendulum arm	L_A	0.086 m
Length of pendulum link	L_L	0.128 m)
Inertia moment of pendulum arm	J_A	5.72×10^{-5} kg m ²
Inertia moment of pendulum link	J_L	1.31×10^{-4} kg m ²
Damping ratio of the rotary pendulum	ζ_P	0.367
Natural frequency of the rotary pendulum	ω_{nP}	11.12 Hz
Damping ratio of encoder cable oscillation	ξ_{n_cableP}	0.034
Natural frequency of encoder cable oscillation	ω_{n_cableP}	10.36 Hz

for the effect of encoder cable. Disturbance from the encoder cable is also a certain factor which influences optimal energy in the swing-up process of the 2DOF QUBE-pendulum.

Acknowledgments

This work was supported by The University of Danang, University of Science and Technology, code number of Project: T2020-02-02.

Manuscript received by Editorial Board, July 03, 2020;
final version, September 24, 2020.

References

- [1] H. Hjalmarsson. System identification of complex and structured systems. *European Journal of Control*, 15(3-4): 275–310, 2019. doi: [10.3166/ejc.15.275-310](https://doi.org/10.3166/ejc.15.275-310).
- [2] L. Ljung. *System Identification: Theory for the User*. 2nd edition, Pearson, 1998.
- [3] P.V. Dang, S. Chatterton, P. Pennacchi, and A. Vania. Numerical investigation of the effect of manufacturing errors in pads on the behaviour of tilting-pad journal bearings. *Proceedings of the Institution of Mechanical Engineers, Part J: Journal of Engineering Tribology*, 232(4):480–500, 2018. doi: [10.1177/1350650117721118](https://doi.org/10.1177/1350650117721118).
- [4] P.V. Dang, S. Chatterton, and P. Pennacchi. The effect of the pivot stiffness on the performances of five-pad tilting pad bearings. *Lubricants*, 7(7):61, 2019. doi: [10.3390/lubricants7070061](https://doi.org/10.3390/lubricants7070061).
- [5] S. Chatterton, P. Pennacchi, A. Vania, and P.V. Dang. Cooled pads for tilting-pad journal bearings. *Lubricants*, 7(10):92, 2019. doi: [10.3390/lubricants7100092](https://doi.org/10.3390/lubricants7100092).
- [6] S. Chatterton, P. Pennacchi, A. Vania, A. De Luca, and P.V. Dang. Tribo-design of lubricants for power loss reduction in the oil-film bearings of a process industry machine: Modelling and experimental tests. *Tribology International*, 130:133–145, 2019. doi: [10.1016/j.triboint.2018.09.014](https://doi.org/10.1016/j.triboint.2018.09.014).
- [7] M.Q. Phan and J.A. Frueh. System identification and learning control. In: Z. Bien, J-X. Xu, editors, *Iterative Learning Control*, chapter 15, pages 285–310. Springer, Boston, MA, 1998. doi: [10.1007/978-1-4615-5629-9_15](https://doi.org/10.1007/978-1-4615-5629-9_15).
- [8] C. Shrivankumar and R. Tiwari. Experimental identification of cracked rotor system parameters from the forward and backward whirl responses. *Archive of Mechanical Engineering*, 66(3):329–353, 2019. doi: [10.24425/ame.2019.129679](https://doi.org/10.24425/ame.2019.129679).
- [9] D.K. Roy and R. Tiwari. Development of identification procedure for the internal and external damping in a cracked rotor system undergoing forward and backward whirls. *Archive of Mechanical Engineering*, 66(2):229–255, 2019. doi: [10.24425/ame.2019.128446](https://doi.org/10.24425/ame.2019.128446).
- [10] A. Wadi, J. Lee, and L. Romdhane. Nonlinear sliding mode control of the Furuta pendulum. *2018 11th International Symposium on Mechatronics and its Applications (ISMA)*, Sharjah, United Arab Emirates, 4–6 March 2018. doi: [10.1109/ISMA.2018.8330131](https://doi.org/10.1109/ISMA.2018.8330131).
- [11] J.L.D. Madrid, E.A.G. Querubín, and P.A. Ospina-Henao. Predictive control of a Furuta pendulum. *2017 IEEE 3rd Colombian Conference on Automatic Control (CCAC)*, Cartagena, Colombia, 18–20 October, 2017. doi: [10.1109/CCAC.2017.8276483](https://doi.org/10.1109/CCAC.2017.8276483).
- [12] I. Paredes, M. Sarzosa, M. Herrera, P. Leica, and O. Camacho. Optimal-robust controller for Furuta pendulum based on linear model. *2017 IEEE Second Ecuador Technical Chapters Meeting (ETCM)*, Salinas, Ecuador, 16–20 October, 2017. doi: [10.1109/ETCM.2017.8247510](https://doi.org/10.1109/ETCM.2017.8247510).

- [13] M. Antonio-Cruz, R. Silva-Ortigoza, J. Sandoval-Gutiérrez, C.A. Merlo-Zapata, H. Taud, C. Márquez-Sánchez, and V.M. Hernández-Guzmán. Modeling, simulation, and construction of a Furuta pendulum test-bed. *2015 International Conference on Electronics, Communications and Computers (CONIELECOMP)*, pages 72–79, Cholula, Mexico, 25–27 February, 2015. doi: [10.1109/CONIELECOMP.2015.7086928](https://doi.org/10.1109/CONIELECOMP.2015.7086928).
- [14] P.X. La Hera, L.B. Freidovich, A.S. Shiriaev, and U. Mettin. New approach for swinging up the Furuta pendulum: Theory and experiments. *Mechatronics*, 19(8):1240–1250, 2009. doi: [10.1016/j.mechatronics.2009.07.005](https://doi.org/10.1016/j.mechatronics.2009.07.005).
- [15] K. Furuta and M. Iwase. Swing-up time analysis of pendulum. *Bulletin of the Polish Academy of Sciences: Technical Sciences*, 52(3):153–163, 2004.
- [16] K. Andrzejewski, M. Czyżniewski, M. Zielonka, E. Łangowski, and T. Zubowicz. A comprehensive approach to double inverted pendulum modelling. *Archives of Control Sciences*, 29(3):459–483, 2019. doi: [10.24425/acs.2019.130201](https://doi.org/10.24425/acs.2019.130201).
- [17] M. Gäfvert, J. Svensson, and K.J. Astrom. Friction and friction compensation in the Furuta pendulum. *1999 European Control Conference (ECC)*, pages 3154–3159, Karlsruhe, Germany, 31 August – 3 September, 1999. doi: [10.23919/ECC.1999.7099812](https://doi.org/10.23919/ECC.1999.7099812).
- [18] *QUBE-servo Experiment for LabVIEW Users*. Student book. Quanser System, 2014.
- [19] A. Kathpal and A. Singla. SimMechanics™ based modeling, simulation and real-time control of Rotary Inverted Pendulum. *2017 11th International Conference on Intelligent Systems and Control (ISCO)*, pages 166–172, Coimbatore, India, 5–6 January, 2017. doi: [10.1109/ISCO.2017.7855975](https://doi.org/10.1109/ISCO.2017.7855975).
- [20] D.L. Peters. Design of a higher order attachment for the Quanser Qube. *2016 American Control Conference*, pages 6634–6639, Boston, USA, 6–8 July, 2016. doi: [10.1109/ACC.2016.7526715](https://doi.org/10.1109/ACC.2016.7526715).
- [21] R.M. Reck. Validating DC motor models on the Quanser Qube Servo. In: *Proceedings of the ASME 2018 Dynamic Systems and Control Conference (DSCC2018)*, V002T16A005, Atlanta, USA, 30 September–3 October, 2018. doi: [10.1115/DSCC2018-9158](https://doi.org/10.1115/DSCC2018-9158).
- [22] Y.V. Hote. Analytical design of lead compensator for Qube Servo system with inertia disk: An experimental validation. *2016 2nd International Conference on Contemporary Computing and Informatics (IC3I)*, pages 341–346, Noida, India, 14–17 December 2016. doi: [10.1109/IC3I.2016.7917986](https://doi.org/10.1109/IC3I.2016.7917986).
- [23] N. Krishnan. *Estimation and Control of the Nonlinear Rotary Inverted Pendulum: Theory and Hardware Implementation*. M.Sc. Thesis, San Diego State University, San Diego, USA, 2019.
- [24] A. Bisoi, A.K. Samantaray, and R. Bhattacharyya. Control strategies for DC motors driving rotor dynamic systems through resonance. *Journal of Sound and Vibration*, 411:304–327, 2017. doi: [10.1016/j.jsv.2017.09.014](https://doi.org/10.1016/j.jsv.2017.09.014).
- [25] G. Bartolini, E. Punta, and T. Zolezzi. Approximability properties for second-order sliding mode control systems. *IEEE Transactions on Automatic Control*, 52(10):1813–1825, 2007. doi: [10.1109/TAC.2007.906179](https://doi.org/10.1109/TAC.2007.906179).